Heliyon 9 (2023) e21054

Contents lists available at ScienceDirect

Heliyon

journal homepage: www.cell.com/heliyon

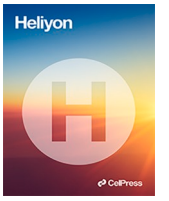

Design, synthesis and anticancer evaluation of polymethoxy aurones as potential cell cycle inhibitors

Zheng Wu [a,1], Yaoyao Han [a,b,1], Xiaolan Li [a,b,1], Qiuping Zhang [b], Renjin Deng [a], Hong Ren [a,b], Wenjing He [a], Xinduo Wu [a], Hongwei Guo [a,b,*], Dan Zhu [a,**]

[a] *Guangxi Key Laboratory of Bioactive Molecules Research and Evaluation & Guangxi Health Commission Key Laboratory of Basic Research on Antigeriatric Drugs, College of Pharmacy, Guangxi Medical University, Nanning, 530021, China*

[b] *Key Laboratory of Longevity and Aging-related Diseases of Chinese Ministry of Education & Center for Translational Medicine, Guangxi Medical University, Nanning, 530021, China*

A R T I C L E I N F O

Keywords:
Polymethoxy aurones
Prostate cancer
Cell cycle
CyclinB1/CDK1 inhibitor
Network pharmacology
Molecular docking
ADMET prediction

A B S T R A C T

Background: Cancer is the most fatal disease in humans and the aberrant activity of various cell cycle proteins results in uncontrolled tumor cell proliferation, thus, regulating the cell cycle is an attractive target in cancer therapy.

Objectives: Aurone is a naturally occurring active compound with a wide range of biological activities, of which 3, 4, 5-trimethoxyphenyl (TMP) is an important microtubule targeting pharmacophore. Based on the pharmacophore combination principle, we incorporate the TMP pharmacophore into the aurone structure and design a novel polymethoxy derivative that is expected to inhibit tumor cell proliferation through regulating the cell cycle.

Methods: By introducing different substituents on C-4′ and C-3′, a series of new 4, 5, 6-trimethoxy aurone derivatives have been designed and synthesized. DU145, MCF-7 and H1299 cell lines were selected to evaluate their anticancer activity. The compound with the best cytotoxicity was then selected and the anticancer mechanisms were investigated by network pharmacology, flow cytometry, Western blot, and cell heat transfer assay. ADMET prediction evaluated the druggability of aurone derivatives.

Results: Aurones **1b** and **1c** have selective anti-proliferative activity against DU145 cells. Among them, the compound **1c** have better cytotoxicity against DU145. Compound **1c** could bind the active cavity of CyclinB1/CDK1/CKS complex protein and induced G2/M phase arrest of DU145 cells by regulating the expression of CyclinB1 and p21. Compound **1c** satisfies the Lipinski rule, is suitable for the absorption and metabolism index, and has a lower risk of cardiac toxicity.

Conclusions: Polymethoxy aurones **1c** might function as a CyclinB1/CDK1 inhibitor that deserved to be further developed for the treatment of prostate cancer.

* Corresponding author. Guangxi Key Laboratory of Bioactive Molecules Research and Evaluation & Guangxi Health Commission Key Laboratory of Basic Research on Antigeriatric Drugs, Key Laboratory of Longevity and Aging-related Diseases of Chinese Ministry of Education & Center for Translational Medicine, Guangxi Medical University, Nanning 530021, China.

** Corresponding author. Guangxi Key Laboratory of Bioactive Molecules Research and Evaluation & Guangxi Health Commission Key Laboratory of Basic Research on Antigeriatric Drugs, College of Pharmacy, Guangxi Medical University, Nanning 530021, China.

E-mail addresses: hongweiguo@gxmu.edu.cn (H. Guo), zdgxmu2006@163.com (D. Zhu).

[1] Zheng Wu, Yaoyou Han and Xiaolan Li are contributed equally to this work.

https://doi.org/10.1016/j.heliyon.2023.e21054
Received 31 May 2023; Received in revised form 11 October 2023; Accepted 13 October 2023
Available online 14 October 2023

1. Introduction

Nowadays, cancer is the most fatal disease in humans, and the incidence and mortality are sharply growing in each year. Aberrant activity of various cell cycle proteins results in uncontrolled tumor cells proliferation, therefore, regulating the cell cycle is an attractive target in cancer therapy [1].

Aurones (2-benzylidenebenzofuran-3(2*H*)-ones), which are structurally isomeric of flavonoids, is the main ingredient conferring to some bright golden flowers [2]. Aurones have been reported to show abroad bioactivities, such as antitumor [3], antioxidative [4], and antiviral [5] activities. Especially, aurone is a novel skeleton as an anticancer agent inhibiting the DNA strand-scission, topoisomerase, cyclin-dependent kinase (CDKs) and tubulin polymerization activities [6]. Moreover, the 3, 4, 5-trimethoxyphenyl (TMP) is also an important moiety in microtubule-targeting agents (MTAs), such as combretastatin A-4 (CA-4) have achieved significant success in the treatment of cancer. [7,8] Following the pharmacophore combination principle, we introduced three trimethoxy groups into the A-ring of the aurone and added different groups in the B-ring to design a series of novel anti-tumor molecules that are expected to inhibit tumor cell proliferation through the cell cycle (Fig. 1).

2. Materials and methods

2.1. General information

Melting points were determined using X-5 digital display binocular microscope (uncorrected). ^{1}H NMR and ^{13}C NMR spectra were recorded on a Bruker Avance III HD600 (600 MHz) spectrometer; *J* values are in Hz. Mass spectra (Water Xevo G2-XS qTOF) were recorded on an electro-spray ionization mass spectrometer as the value *m/z*.

Western blot on the membrane were developed with the ECL system (Thermo Fisher, USA) and images were captured using the Odyssey infrared imaging system (LI-COR Biosciences, USA). Band intensity was quantified by densitometric analysis using Image Studio Lite software (LI-COR Biosciences, USA). Cell cycle distribution was evaluated using a flow cytometer (BD LSR Fortessa, Becton Dickinson & Co., USA).

Human prostate cancer (DU145), breast cancer (MCF-7) and lung cancer (H1299) cell lines were obtained from the Cell Bank of the Chinese Academy of Science (Shanghai, China). Phosphate buffered saline (PBS), Roswell Park Memorial Institute (RPMI)-1640 medium, Dulbecco's modifcation of Eagle's medium (DMEM) medium, penicillin/streptomycin, and antibiotics were purchased from Beijing Vicente Biotechnology Co., Ltd. (Beijing, China). Dimethyl sulfoxid (DMSO) was obtained from Sigma-Aldrich (St.Louis, MO, USA). Fetal calf serum (FBS) was obtained from Gibco (Grand Island, NY, USA). Cell Counting Kit-8 (CCK-8) Assay Kit was obtained from Boster Biological Technology co. Itd (Wuhan, China). Cell Cycle Kit was purchased from BD Biosciences (San Jose, CA, USA). Radioimmunoprecipitation assay (RIPA) buffer were purchased from Thermo Fisher Scientifc (Waltham, USA). BCA (Bicinchoninic Acid) Protein Assay Kit was purchased from Beyotime Biotechnology Co., Ltd. (Shanghai, China). PVDF (polyvinylidene fluoride) membranes purchase from Millipore, USA. All the primary antibodies such as p21, CDK1, CyclinB1 and GAPDH (glyceraldehyde-3-phosphate dehydrogenase) were purchased from Cell Signaling Technology (Danvers, USA).

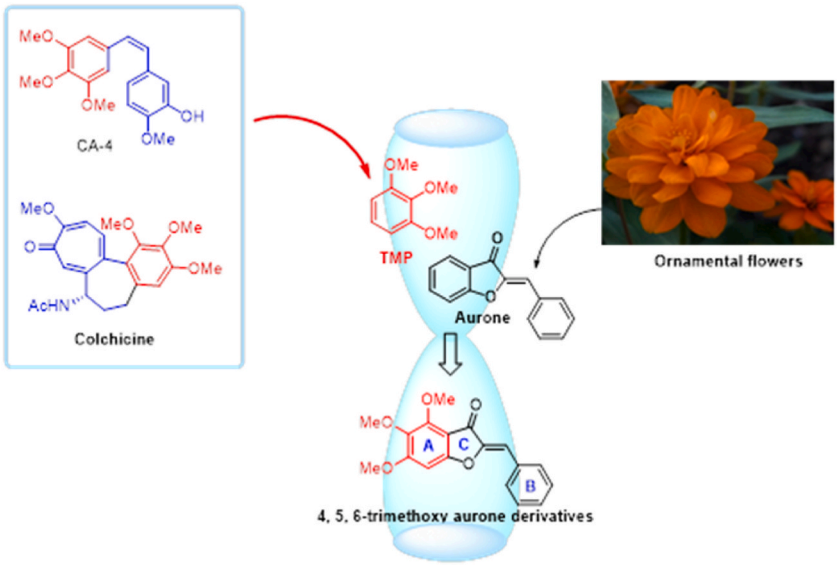

Fig. 1. The design of 4, 5, 6-trimethoxy aurone derivatives through the pharmacophore combination principle.

2.2. Chemistry

2.2.1. General procedure for the synthesis of aurones (compound **1**)

To a solution of **2** (51.2 mg, 0.23 mmol) in methanol (10 mL) was added 80 % KOH (0.08 mL). The solution was stirred at room temperature for 0.5 h. Then, substituted benzaldehyde (0.76 mmol) was added dropwise, and the mixture refluxed for 1–30 h (monitored by TLC). Cooled to room temperature, remove methanol under reduced pressure. Added water to the residue, and acidized by HCl, then precipitate appears. Filtered the solid under vacuum to give the crude product. The crude product was purified by recrystallization or silica column chromatography [9].

2.2.2. (Z)-2-(4-hydroxybenzylidene)-4,5,6-trimethoxybenzofuran-3(2H)-one (compound **1a**)

Silica column chromatography (EtOAc/petroleum ether, *v/v*, 1:4) to give yellow solids, yield 68.2 mg (90.4 %), mp 204–205 °C. ^{1}H NMR (600 MHz, $CDCl_3$) δ, ppm *(J,* Hz*)*: 3.85(3H, s, –OCH_3), 4.00(3H, s, –OCH_3), 4.28(3H, s, –OCH_3), 6.57(1H, s, Ph-H), 6.77(1H, s, –CH), 6.93–6.94(2H, d, J = 6.0 Hz, Ph-H), 7.81–7.82(2H, d, J = 6.0 Hz, Ph-H). ^{13}C NMR (150 MHz, $CDCl_3$) δ, ppm: 180.98, 163.85, 161.56, 157.55, 151.61, 146.51, 136.59, 133.28, 125.03, 116.03, 111.93, 107.34, 90.55, 62.38, 61.66, 56.63. Found, *m/z*: 329.1020 $[M+H]^+$. $C_{18}H_{16}O_6$, Calculated, *m/z*: 329.1028.

2.2.3. (Z)-2-(3-chloro-4-hydroxybenzylidene)-4,5,6-trimethoxybenzofuran-3(2H)-one (compound **1b**)

Silica column chromatography (EtOAc/petroleum ether, *v/v*, 1:4) to give yellow solids, yield 35.8 mg (43.0 %), mp 193–194 °C. ^{1}H NMR (600 MHz, $CDCl_3$) δ, ppm *(J,* Hz*)*: 3.85(3H, s, –OCH_3), 4.02(3H, s, –OCH_3), 4.28(3H, s, –OCH_3), 6.60(1H, s, Ph-H), 6.68(1H, s, –CH), 7.10–7.11(1H, d, J = 12.0, Ph-H), 7.67–7.69(1H, d, J = 12.0, Ph-H), 7.95(1H, s, Ph-H). ^{13}C NMR (150 MHz, $CDCl_3$) δ, ppm: 180.65, 163.88, 161.70, 152.42, 151.73, 147.08, 136.72, 131.81, 131.47, 126.35, 120.55, 116.65, 109.83, 107.07, 90.62, 62.40, 61.65, 56.69. Found, *m/z*: 363.0630 $[M+H]^+$. $C_{18}H_{15}ClO_6$, Calculated, *m/z*: 363.0634.

2.2.4. (Z)-2-(3-bromo-4-hydroxybenzylidene)-4,5,6-trimethoxybenzofuran-3(2H)-one (compound **1c**)

Silica column chromatography (EtOAc/petroleum ether, *v/v*, 2:7) to give yellow solids, yield 39.2 mg (42.0 %), m. p. 207–208 °C. ^{1}H NMR (600 MHz, $CDCl_3$) δ, ppm *(J,* Hz*)*: 3.82(3H, s, –OCH_3), 4.00(3H, s, –OCH_3), 4.27(3H, s, –OCH_3), 6.57(1H, s, Ph-H), 6.65(1H, s, –CH), 7.07–7.09(1H, d, J = 12.0, Ph-H), 7.70–7.71(1H, d, J = 6.0, Ph-H), 8.01(1H, s, Ph-H). ^{13}C NMR (150 MHz, $CDCl_3$) δ, ppm: 180.61, 163.88, 161.68, 153.25, 151.73, 147.08, 136.73, 134.49, 132.48, 126.82, 116.43, 110.84, 109.60, 107.07, 90.63, 62.41, 61.65, 56.70. Found, *m/z*: 407.0125 $[M+H]^+$. $C_{18}H_{15}BrO_6$, Calculated, *m/z*: 407.0134.

2.2.5. (Z)-2-(4-bromobenzylidene)-4,5,6-trimethoxybenzofuran-3(2H)-one (compound **1d**)

Recrystallized from ethanol to afford compound **1d**, yellow solids, yield 43.2 mg (48.0 %), mp 187–189 °C. ^{1}H NMR (600 MHz, $CDCl_3$) δ, ppm *(J,* Hz*)*: 3.82(3H, s, –OCH_3), 3.99(3H, s, –OCH_3), 4.25(3H, s, –OCH_3), 6.55(1H, s, Ph-H), 6.69(1H, s, –CH), 7.55–7.56 (2H, d, J = 6.0 Hz, Ph-H), 7.71–7.73(2H, d, J = 12.0 Hz, Ph-H). ^{13}C NMR (150 MHz, $CDCl_3$) δ, ppm: 180.77, 163.82, 161.41, 160.69, 151.65, 146.61, 136.60, 132.96, 125.28, 114.40, 111.49, 107.31, 90.52, 62.42, 61.64, 56.61. Found, *m/z*: 391.0176 $[M+H]^+$. $C_{18}H_{15}BrO_5$, Calculated, *m/z*: 391.0183.

2.2.6. (Z)-2-(4-fluorobenzylidene)-4,5,6-trimethoxybenzofuran-3(2H)-one (compound **1e**)

Recrystallized from ethanol to afford compound **1e**, yellow solids, yield 20.0 mg (25.0 %), mp 202–203 °C. ^{1}H NMR (600 MHz, $CDCl_3$) δ, ppm *(J,* Hz*)*: 3.85(3H, s, –OCH_3), 4.01(3H, s, –OCH_3), 4.28(3H, s, –OCH_3), 6.57(1H, s, Ph-H), 6.76(1H, s, –CH), 7.14–7.17 (2H, t, J = 6.0 Hz, Ph-H), 7.88–7.90(2H, m, Ph-H). ^{13}C NMR (150 MHz, $CDCl_3$) δ, ppm: 180.75, 164.02, 164.00, 162.33, 161.73, 151.78, 147.35, 147.33, 136.73, 133.11, 133.05, 128.83, 128.81, 116.09, 115.95, 110.00, 107.01, 90.54, 62.41, 61.64, 56.67. Found, *m/z*: 331.0976 $[M+H]^+$. $C_{18}H_{15}FO_5$, Calculated, *m/z*: 331.0982.

2.3. Biological experiments

Microtubule-targeting inhibitors such as paclitaxel are broad-spectrum anti-tumor drugs which commonly used to treat solid tumors such as breast cancer, prostate cancer and lung cancer etc. For the past few years, we have focused our research efforts on screening antitumor drugs from natural products [10,11].

DU145 is an androgen independent cell with low differentiation and moderate metastatic potential and is considered as a standard prostate cancer cell line for therapeutic research [12]. Our previous studies showed that *Marsdenia tenacissima* (Roxb.) moon injection induced apoptosis of DU145 cell by regulating AKT/GSK3β/STAT3 signaling axis and exerted a potential anti-tumor effect in prostate cancer through inhibiting ErbB2-GSK3β-HIF1α signaling axis, which may be related to the tricarboxylic acid cycle [13,14]. Total flavonoids of Litchi seed attenuated the progression of prostate cancer including DU145 cells via inhibiting AKT/mTOR and NF-κB signaling pathways [15,16].

Breast cancer is the leading invasive cancer in women globally, being estrogen receptor-positive (ER+) the most common subtype [17]. MCF-7 is an estrogen receptor positive cell and retains multiple differentiated mammary epithelial characteristics [18,19]. Our previous studies revealed that chlorogenic acid inhibited epithelial-mesenchymal transition and invasion of MCF-7 cell by down-regulating LRP6 [20]. Total flavonoids of Litchi seed attenuated stem cell-like properties of breast cancer through reducing the percentage of $CD44^+CD24^-$/low cells, inhibiting the mammospheres formation and down-regulating the mRNA and protein levels of cancer stem cells related markers in MCF-7 cells by regulating Notch3 signaling pathway [21].

H1299 is an Non-small cell lung cancer cell line with p53-null [22] and is widely used in a variety of basic cell biology and biomedical studies, involving lung cancer proliferation, cell apoptosis, cell cycle [23], metastasis [24], and the development of inhibitors [25, 26, 27].

Therefore, in this paper, prostate cancer, breast cancer and lung cancer cell lines (DU145, MCF-7 and H1299) were selected for biological experiments.

2.3.1. Cell proliferation assay

DU145, MCF-7 and H1299 cell lines were cultured in RPMI-1640 media or DMEM media supplemented with 10 % FBS, 1 % penicillin/streptomycin and incubated in a 5 % CO_2 humidified atmosphere at 37 °C. CCK-8 assay was performed to assess cell proliferation ability followed the previous study [14]. DMSO was used as the mother liquor, and different concentrations of the solution were diluted with a complete medium. The absorbance values were measured at 450 nm. The Dose-response curves generation and IC_{50} values calculation were performed by GraphPad Prism 7 [28]. The cytotoxic effects of the synthesized compounds on DU145, MCF-7 and H1299 cells were evaluated by CCK-8 method. The general procedure is as follows: cells are seeded in 96-well plates (2000–2500 cells/well) overnight, and then incubated with the compounds (**1a-1e**) at different concentrations (0.1–320 μM). After treatment for 72 h, the CCK-8 reagent was added to the culture medium and incubated with the cells for an additional 0.5 h. Absorbance was measured by a microplate reader (Thermo, USA) at 450 nm (OD1 means the optical density value in medicine groups, OD2 means the average optical density value in all duplicates in the control group). The relative cell viability in percentage was calculated as follows:

$$\text{Relative cell viability } (\%) = \frac{\text{OD1}}{\text{OD2}} \times 100\ \%$$

2.3.2. Network pharmacology

Disease-related target genes were obtained from GeneCards Database (https://www.genecards.org/)[29, 30], and the targets of compound were predicted by ChemMapper Database (http://lilab-ecust.cn/chemmapper/) [31]. Cytoscape software (version 3.2.1) was applied to graphically display the network of compound, disease and the targets interacting with them [32]. FunRich (version 3.1.3) was used for drawing a Venn diagram of targets both compound and disease related. To further explore the biological processes of the candidate compound involved, Kyoto Encyclopedia of Genes and Genomes (KEGG) pathway enrichment analysis (http://www.kegg.jp/) was applied to screen the top signal pathways based on the *P*-value.

2.3.3. Cell cycle assay

The DU145 cells were seeded into a cell culture dish (6 cm in diameter) at a density of 2.5×10^5 cells/mL and incubated for 24 h at 37 °C and 5 % CO_2. Then, the medium was removed and replaced with a medium (DMSO 0.5 % *v/v*) containing 5 or 10 μM of compound **1c**. After treatment for 72 h, the cell layer was trypsinized and washed with ice-cold phosphate buffered saline (PBS), fixed with 75 % ice-cold ethanol for overnight. The fixed cells were rinsed with PBS and then stained with the DNA fluorochrome 7-AAD in a solution containing stain buffer under dark condition for 15 min at 37 °C according to the instruction manual. Then samples were detected by flow cytometry (Accuri C6 Plus, BD Biosciences, United States).

2.3.4. Western blot analysis

The DU145 cells treated with compound **1c** were lysed on ice using RIPA buffer to obtain total protein. Lysates were centrifuged at 12000 rpm for 15 min at 4 °C. The protein concentration was determined by a BCA protein assay kit. 40 μg of denatured protein samples was separated by SDS-PAGE (10 %–15 %) and transferred onto PVDF membranes. The PVDF membranes were further blocked with 5 % non-fat milk at room temperature for 1 h and then incubated with specific primary antibodies [p21, CDK1, CyclinB1 (working concentration 1:1000)] diluted in 1 × PBS at 4 °C overnight. After three washes with Tris-buffered saline Tween (TBST) for 15 min, the membranes were incubated with secondary antibodies (Anti-mouse IgG,1:30000). The results were presented as a percentage of the internal control GAPDH.

2.3.5. Molecular docking

Surflex-dock of SYBYL-X 2.0 software (Tripos Inc., St Louis, USA) was used to study the interaction between CyclinB1/CDK1/CKS and compound **1c**. A ternary complex of human proteins CDK1/Cyclin B/CKS2 (PDB code:5HQ0 [33]) was selected and downloaded from the RCSB Protein Data Bank (https://www.rcsb.org/) [34], that the resolution is 2.30 Å.

Several protein preparation works were done before using the docking programs. Firstly, the molecular structure of compound **1c** was optimized through the standard Tripos force field with a 0.005 kcal (mol Å)$^{-1}$ energy gradient convergence criterion and using Gasteiger–Hückel charges to calculate the partial atomic charges. The structural energy minimizations were performed using the Powell method 10000 iterations. The other parameters were set as default values in SYBYL-X 2.0 software. Secondly, the original ligand was extracted from the active site of the protein and all water molecules were removed from the original protein complex. Next, protein analysis and repair were carried out following the procedure demands, such as repair sidechain, termini treatment by charges state, set acids residues protonation type near ligands, added hydrogens, added charge by AMBER7 FF99 biopolymer and Gasteiger-Hückel ligands, fixed sidechain amides and staged minimization (minimization parameters were the same as molecular structure minimization). Afterward, the ProtoMol file was generated by the ligand-based docking mode and each structure was docked into the active pocket using surflex-dock. In addition, the co-crystallized ligand was set as a reference molecule during the docking simulation.

Based on the similarity of the orientation between the original ligand and the conformations, the conformation with the highest docking score was chosen for the study of the binding mode.

2.3.6. Cellular thermal shift assay (CETSA)

DU145 cells were lysed by RIPA containing protease inhibitors and total proteins were collected. Cell lysates were centrifuged at 12,000 rpm for 20 min, the supernatant was equally divided into two parts, with one part treated with DMSO and the other part treated with **1c** (200 μM). After incubation at room temperature for 1 h, the two parts were divided into seven aliquots (50 μL) respectively, then heated at temperatures of 37, 42, 47, 52, 57, 62, and 67 °C for 3 min. Afterward, every aliquot was centrifuged and the supernate was analyzed by Western blot.

2.3.7. Pharmacokinetics and drug likeness prediction

A successful drug should satisfy in biochemical properties, pharmacokinetics and safety. High potency and selectivity, desirable absorption, distribution, metabolism, excretion and toxicity (ADMET) characteristics were the important conditions for the success of a drug candidate [35, 36, 37]. Therefore, it is necessary to acknowledge the ADMET properties of the designed compounds in advance. We use the ADMET Evaluation function of ADMETlab 2.0 (https://admetmesh.scbdd.com/) to predict their ADMET properties [38].

The chemical structure of the compound is plotted in the web tool and then submitted. The analysis of absorption, distribution, metabolism, excretion and toxicity properties, including Lipinski rules were well measured by the following paraments: Pgp-inhibitor, Human Intestinal Absorption (HIA), 30 % Bioavailability ($F_{30\ \%}$), Plasma Protein Binding (PPB), Blood-Brain Barrier (BBB) Penetration, CYP1A2 inhibitor, CYP1A2 substrate, Clearance (CL), half-life ($T_{1/2}$), hERG Blockers and rat oral acute toxicity, and so on. Finally, this web tool was used to evaluate the drug-likelihood of aurone derivative **1c**, including the Lipinski rule and bioavailability.

2.3.8. Statistical analysis

Dates were presented as means ± SD and analyzed by one-way-ANOVA by SPSS version 24.0. Results are considered as statistical significance when $p < 0.05$.

3. Results and discussion

3.1. Chemistry

In this paper, the benzofuranones intermediate approach was selected to synthesize polymethoxy aurones, which were easily prepared from commercially available 3, 4, 5-trimethoxy benzaldehyde (see Scheme 1).

In this process, Dakin oxidation was first applied to synthesize compound **4** from 3, 4, 5-trimethoxybenzaldehyde. After the reaction, $NaHCO_3$ was added to neutralize the by-product 3-chlorobenzoic acid, which gives a good yield. Compound **4** was reacted with potassium hydroxide in methanol to produce 3, 4, 5-trimethoxyphenol within 5 min, otherwise the by-products appear and increase in quantity over time. Then, potassium carbonate/acetone system was applied to replace KOH or Na in the substitution reaction between 3, 4, 5-trimethoxyphenol and 2-chloroethylene acetate with good yields. Esterolysis reactions take place in the NaOH/EtOH system to obtain compound **3** without purification. Compound **2** was cycling from compound **3** through polyphosphoric acid (PPA) catalyze in anhydrous condition. The single geometric isomer (*Z*) compound **1** was prepared from compound **2** by KOH catalyzed condensation with an appropriate aldehyde, because of an intermolecular hydrogen bond between carbonyl and methine, which is generally more thermodynamically stable than the (*E*)-isomer [39].

3.2. Biological evaluation

3.2.1. In vitro anti-proliferative activity

All of the synthesized compounds were screened by the CCK-8 assay. Prostate cancer (DU145), breast cancer (MCF-7) and lung cancer (H1299) cell lines were selected to screen for anti-proliferative activities, and the results showed in Table 1 and Fig. 2.

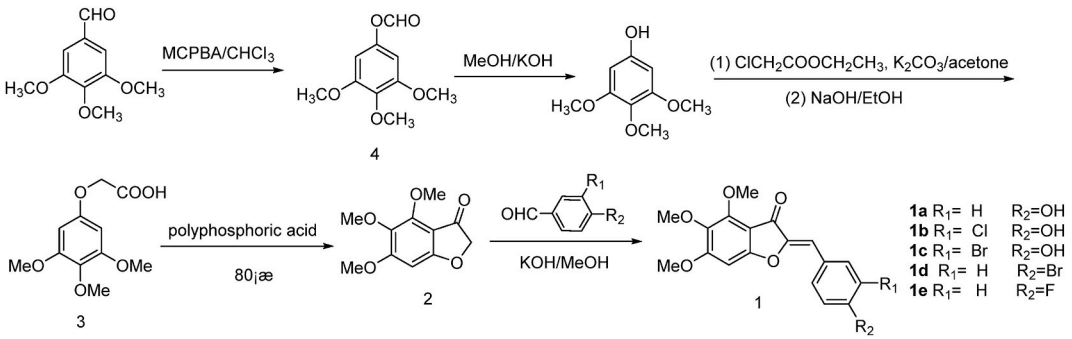

Scheme 1. Synthesis of polymethoxy aurones.

Table 1
The IC_{50} values of synthesized compounds on three cancer cells.

	IC_{50} (μM)		
	DU145	MCF-7	H1299
1a	–	218.67	517.51
1b	37.68	57.04	> 1000
1c	15.56	104.38	> 1000
1d	933.89	941.51	> 1000
1e	>1000	814.07	> 1000

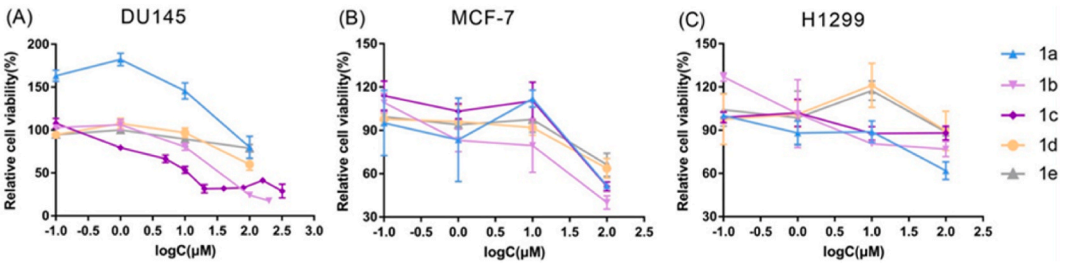

Fig. 2. *In vitro* cytotoxicity analysis of the synthesized compounds against three different human cancer cell lines.

Compared with the MCF-7 and H1229 cell lines, compound 1**b** and 1**c** still have certain inhibition ability below the concentration of 50 μM and showed a certain degree of selectivity in DU145 cells. Then, the structure-activity relationship of aurone analogues in prostate cancer was discussed.

The results of the CCK-8 assay revealed that the introduction of halogen into the C ring enhance the anti-prostate cancer activity. Compound **1a** has only one hydroxyl group on the C ring, which may be responsible for the lack of cytotoxicity in the DU145 cell line. In addition, the hydroxyl group may be synergistic with the halogen group of aurones, as compound **1b** and **1c** with both hydroxyl and halogen groups achieve better anti-prostate cancer activity than compound **1d** and **1e** with only the halogen group in the C ring.

Based on the above results, compound **1c** showed the best anti-proliferative activity with IC_{50} = 15.56 μM. Compound **1c** was selected for further biological evaluation to reveal its anti-prostate cancer mechanism.

3.2.2. Network pharmacology study

Network pharmacology studies have been applied to predict the anti-prostate cancer targets of polymethoxy aurones. Compound **1c**, the most cytotoxicity compound, was used for prediction. As Fig. 3A showed, a total of 20 potential targets of compound **1c** were predicted by the ChemMapper database with the property of "Homo sapiens" set. Then, the GeneCards database was used for searching prostate cancer-related genes and ultimately 2130 genes (Fig. 3B) were retrieved according to the screening criteria of containing the keyword "prostate cancer" and a relevance score greater than or equal to 5. As shown in the Venn diagram of Fig. 3C, the 14 overlapped targets (both **1c** and prostate cancer-related) were identified as key targets for the anti-cancer activity of **1c** for prostate cancer. To further shed light on the biological mechanism of **1c** against prostate cancer, KEGG pathway enrichment analysis was performed based on the 14 common targets with a cut-off *P*-value of 0.05 and count-value of 3.

Finally, the top 5 potential pathways were selected and shown in Fig. 3D, which mainly include the thyroid hormone signaling pathway, measles, herpes simplex infection, prolactin signaling pathway, and cell cycle. Among the pathways, the cell cycle pathway appears to be closely related to the occurrence and development of tumors and has been identified as a prominent pathway for **1c** against DU145 cells. Based on the above results, we design the cell cycle experiments to verify our hypothesis.

3.2.3. Effect on cell cycle progression

To investigate the impact of compound **1c** on the cell cycle progression, DU145 cells were treated with compound **1c** (5 and 10 μM) for 72 h and cell cycle distribution was assessed by 7-AAD-based flow cytometric analysis. As the results shown in Fig. 4A and B, significant changes in cell cycle characteristics of DU145 cells were observed after compound **1c** treatment. In comparison with untreated control cells, the percent of cells at G0/G1 phase showed slightly decrease while the percentage of cells at G2/M treated with 5 μM or 10 μM of **1c** were 31.36 % and 39.17 %, respectively, which were markedly increased. From the above studies, we can infer that compound **1c** arrested the cell cycle at G2/M phase leading to anti-proliferative activity against prostate cancer.

Growing evidence has demonstrated that cyclin-dependent kinases (CDKs) participated the regulation of DNA synthesis and phosphorylation process, and the CyclinB1/CDK1 complex was verified to modulate the transition of the cell cycle from G2 to M phase. [40, 41, 42] Hence, we further assessed the molecular mechanisms underlying the cell cycle arrest induced by compound **1c** in DU145 cells. Several key proteins involved in the progression of G2/M in DU145 cells were then examined by western blotting to confirm that compound **1c** was able to block the G2/M cell cycle to inhibit the proliferation of prostate cancer cell lines. p21 (also known as p21W AF1/Cip1) expression was detected additionally, because this gene is an important inhibitor of CDKs, which could inactivate the

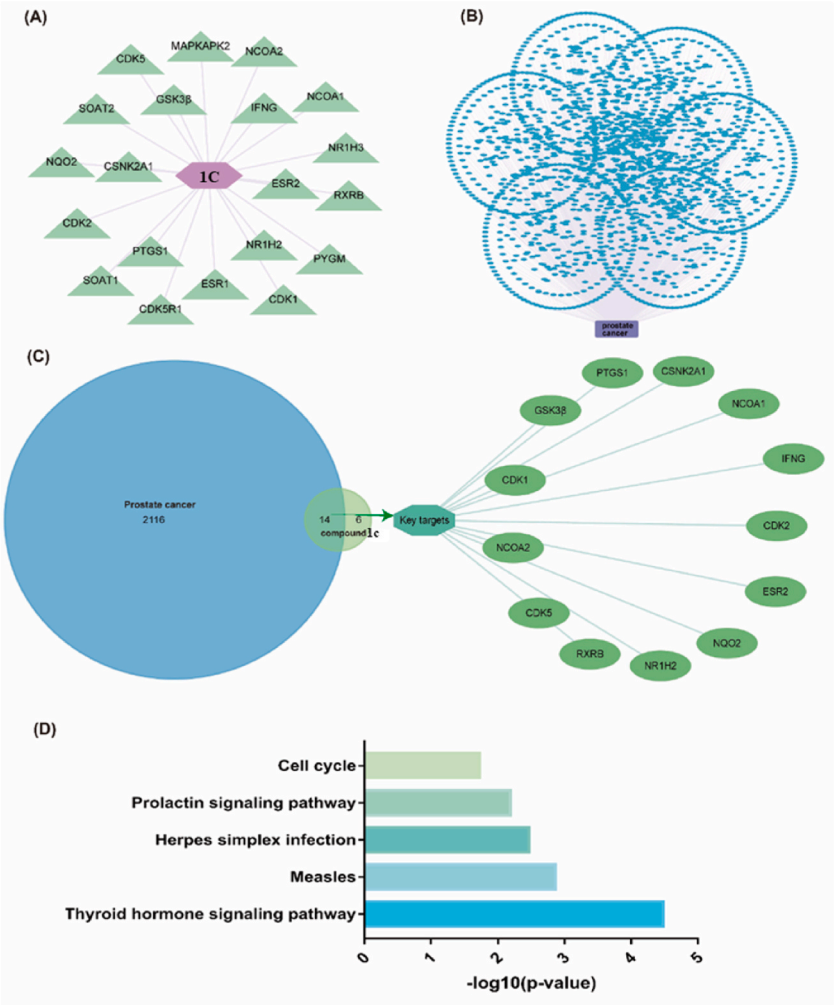

Fig. 3. The analysis of network pharmacology. (A) Compound-target network. The purple node represents compound 1c, the laurel green nodes are targets. (B) Disease-target network. The deep purple rectangle represents prostate cancer, and the blue-black parts are targets. (C) The Venn diagram of the common genes between prostate cancer targets (blue circle) and compound 1c (laurel green circle). (D) The top 5 pathways and their –Log10 (*P*-Value).

CyclinB1/CDK1 complex and then block the cell cycle in the G2/M phase. [43, 44] The results shown in Fig. 4C conform with our expectation that compound **1c** can decrease the expression of CyclinB1 while up-regulated the expression of p21 in a dose-dependent manner, ultimately inducing G2/M-phase arrest.

3.3. Molecular docking

Cyclin B is the only CDK partner of CDK1, both of them can together control the extent of inhibitory phosphorylation within the CDK1 active site with phosphatases [45]. Alternatively, CKS proteins may enhance selective phosphorylation of CDK1 substrates at mitosis, suggesting that the use of the ternary Cyclin B1/CDK1/CKS complex may shed light on synergistic effects in the cell cycle [45]. Therefore, in this paper we employed the ternary complex of human protein (PDB code: 5HQ0) to operate the molecular docking to study the blocking cell cycle mechanism of compound **1c**, expecting to exploit novel CDKs inhibitors in future.

In order to ensure the consistency between the docking model and the co-crystal protein, we first docked the native ligand (ID: LZ9), and the root mean square deviation (RMSD) value between the docked pose and the crystal conformation of the native ligand was found as 0.13 Å, which indicated the docking model was reasonably reliable [46]. Based on this reliable docking model, the docking compound **1c** has a total score of 5.32, which is higher than other aurone derivatives (Table 2).

The CDK1 protein divides into six regions, there are phosphate pocket, ribose pocket, solvent exposed area, DFG area, gatekeeper and hinge area. Among them, hinge area is closely associated with activity [47, 48]. The activation segment in the hinge region can form a platform that recognizes CDK substrate residues to either side of the phosphotransfer site, which is the key factor inhibiting CDK protein [33]. Therefore, lots of CDK inhibitors form hydrogen bonds with this activation segment [49]. When docking with compound

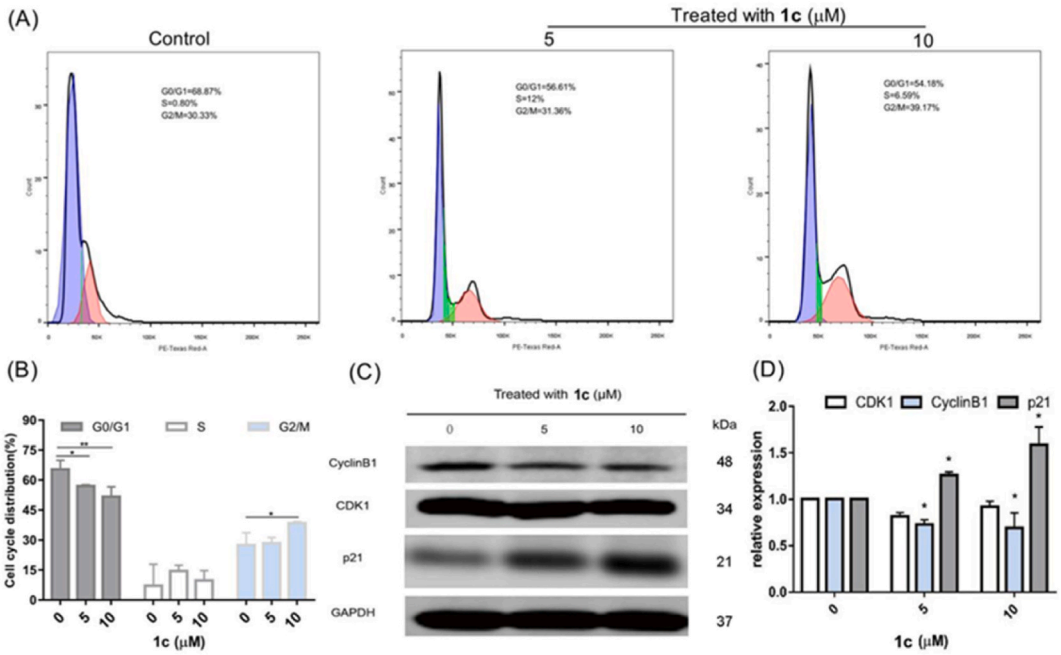

Fig. 4. Compound 1c induced G2/M−phase arrest in DU145 cells. (A) The distribution of cell cycle was monitored using flow cytometry after DU145 cells were treated with compound 1c for 72h. (B) Bar chart depicting the cell cycle distribution in DU145 cells. (C) The expressions of CyclinB1, CDK1, and p21 in DU145 cells were detected by Western blot. GAPDH was used as control. (D) Bar chart showing the relative expression of CyclinB1, CDK1, and p21 in DU145 cells. Data are expressed as mean ± SD, compared with the control group: $^*P < 0.05$.

Table 2
Docking results of aurone derivatives (PDB:5HQ0).

Compounds	1a	1b	1c	1d	1e
Total Score	4.65	4.53	5.32	5.21	5.27

1c, the result (Fig. 5) shows that compound **1c** in the ATP binding pocket forms one hydrogen bond with the amino acid residue LEU83 in the activation segment of CyclinB1/CDK1/CKS protein via the carbonyl group in the core furanone fragment [50]. However, this binding is weaker compared to the native ligand. The native ligand forms not only two hydrogen bonds with LEU83, but also one hydrogen bond with GLU81, which is also in the active segment [51]. Maybe that is the reason why the native ligand obtains a better total score (total score = 7.90) than compound **1c**. In the similar way, except for compound **1c**, other aurone derivatives do not form hydrogen bonds with LEU83 (see supporting materials). It can be concluded that different substitutions on the C ring affect the conformation of the active pocket, and only the appropriate conformation will interact with the active segment to produce biological activity.

Combined with the CCK8, cell cycle assay and molecular docking results, we can infer that compound **1c** is a potential CyclinB1/CDK1 inhibitor that can bind to hinge region of the protein and block the G2/M cell cycle, thereby inhibiting the proliferation of prostate cancer cells.

3.4. Cellular thermal shift assay

Through molecular docking, we have verified that compound **1c** can bind to the Cyclin B1/CDK1/CKS complex protein theoretically, now, CETSA, which is a valuable tool for the validation of drug-target engagement, has applied to confirm the results by practice [52]. Target proteins usually become more stable when they bind to drug molecules. Under general conditions, the protein will be degraded with the increase of temperature, but when the protein binds to the drug, the amount of under-graded protein will increase at the same temperature, so the hot melt curve of the composite protein will shift to the right compared with the solvent control group [53].

Compared with the control group, the degraded temperature of CyclinB1 and CDK1 that binding compound **1c** was raised obviously (Fig. 6). In control group, when the temperature rises to 62 °C, the CyclinB1 degraded observably, and the CyclinB1 composite protein that binding compound **1c** just degraded at the temperature 67 °C. There was the same phenomenon as the CDK1, the degrade temperature of pure CDK1 was approximately 5° lower than its composite protein, whereas the reference protein GAPDH had the same degrade temperature whether composite protein or not. Therefore, these results verified that the compound **1c** has already bonded to

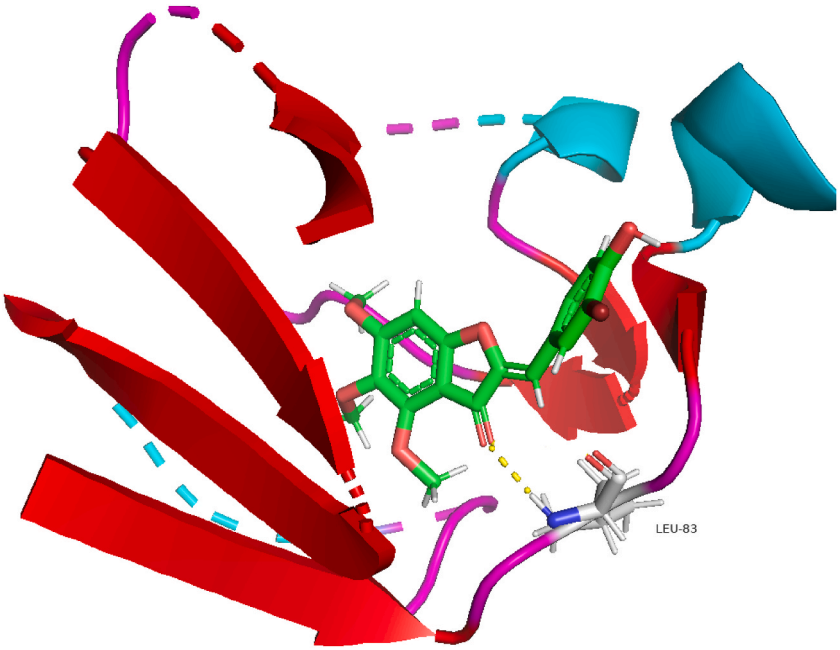

Fig. 5. Molecular docking Interaction of compound 1c with Cyclin B1/CDK1/CKS complex proteins, hydrogen bonds were shown as yellow dotted lines.

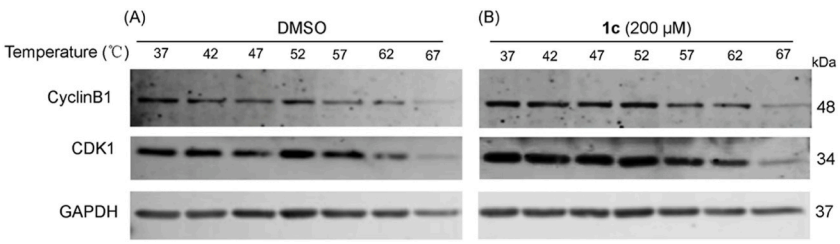

Fig. 6. The 1c-CyclinB1/CDK1 binding was examined in DU145 cells using cellular thermal shift assay and Western blot. The DU145 cells proteins were incubated with (A) DMSO and (B) 1c (200 μM) at room temperature for 1 h.

the CyclinB1/CDK1, and the compound **1c** is a potential CyclinB1/CDK1 inhibitor, however the binding does not tightly enough. This result is consistent with the moderate total score of compound **1c** in molecular docking.

3.5. ADMET prediction

ADMET properties was very important index that evaluated the drug-like properties and pharmacokinetics of drug candidates. We used ADMET lab 2.0 to evaluate the ADMET properties of compound **1c** [54]. The results show that compound **1c** satisfies the Lipinski rule with a molecular weight of 406.01, LogP of 3.237, number of hydrogen bond donors of 1 and number of hydrogen bond acceptors of 6. The absorption is good, except for the Pgp-inhibitor parameter, which is poor, but the other absorption parameters are up to standard. In the distribution, the volume distribution is 0.482, which is in the optimal range where compound **1c** cannot cross the blood-brain barrier. In metabolism, compound **1c** is a CYP1A2 inhibitor to a large extent, reaching a value of 0.942. The closer the value is to one, the more likely it is to be an inhibitor. However, compound **1c** is appropriately a short half-life compound with $T_{1/2}$ of only 0.358 and poor clearance. Compound **1c** had a lower risk of cardiac toxicity, the value is 0.006, and moderate oral acute toxicity in rats with a value of 0.673. A value closer to 0 is more likely to have no toxicity.

The detail of ADMET results please see the supporting information. The ADMET predictions point to future directions of structural modification, with the distribution and excretion terms being the main ones.

4. Conclusion

A convenient method was used to synthesize five 4,5,6-trimethoxy aurone derivatives, and activity screening showed that these polymethoxy aurones had particular inhibitory effect on prostate cancer cells. Structure-activity relationship studies have suggested

that the cytotoxicity of aurone analogues on DU145 cells may be related to a synergistic interaction between the halogen and hydroxyl groups on the C ring. Network pharmacological predictions suggest that polymethoxy aurones **1c** inhibits prostate cancer cells through cell cycles. To verify this finding, we performed cell cycle and Western blot experiments. The results pointed out that the compound **1c** induced G2/M-phase arrest in DU145 cells by regulating the expression of CyclinB1 and p21. Next, we investigate the mechanism of action between CyclinB1/CDK1 and compound **1c**. Combining with molecular docking and CETSA techniques, compound **1c** was found to be able to occupy the ATP binding cavity of CyclinB1/CDK1/CKS, interacting with the key amino residues LEU83 in the activation-segment responsible for influencing the cell cycle of prostate cancer. At last, applied ADMET prediction to evaluate the draggability of compound **1c**. In brief, compound **1c** is a potential CyclinB1/CDK1 inhibitor, and in the future, we can enhance its binding to the active segment of CyclinB1/CDK1/CKS protein, improve its distribution and excretion properties, to develop novel aurone derivative CDK1 inhibitors.

Funding statement

This work was supported by the Guangxi Science and technology project (FANGKE ZY20221502), Guangxi Natural Science Foundation (2020GXNSFAA297114, 2015GXNSFBA139028), and Advanced Innovation Teams and Xinghu Scholars Program of Guangxi Medical University.

Data available

Data included in article/supp. material/referenced in article.

CRediT authorship contribution statement

Zheng Wu: Data curation, Formal analysis, Funding acquisition, Project administration, Software, Writing – original draft, Writing – review & editing. **Yaoyao Han:** Data curation, Investigation, Software, Writing – original draft. **Xiaolan Li:** Data curation, Software, Writing – review & editing. **Qiuping Zhang:** Formal analysis. **Renjin Deng:** Data curation. **Hong Ren:** Data curation. **Wenjing He:** Data curation. **Xinduo Wu:** Data curation, Methodology. **Hongwei Guo:** Conceptualization, Funding acquisition, Project administration, Resources, Supervision, Validation, Writing – review & editing. **Dan Zhu:** Funding acquisition, Project administration, Supervision, Writing – review & editing.

Declaration of competing interest

The authors declare the following financial interests/personal relationships which may be considered as potential competing interests:Hongwei Guo reports financial support was provided by the Advanced Innovation Teams and Xinghu Scholars Program of Guangxi Medical University. Dan Zhu reports financial support was provided by Guangxi Natural Science Foundation (2020GXNSFAA297114). Zheng Wu reports financial support was provided by Guangxi Natural Science Foundation (2015GXNSFBA139028).

Appendix A. Supplementary data

Supplementary data to this article can be found online at https://doi.org/10.1016/j.heliyon.2023.e21054.

References

[1] T. Otto, P. Sicinski, Cell cycle proteins as promising targets in cancer therapy, Nat. Rev. Cancer 17 (2017) 93–115, https://doi.org/10.1038/nrc.2016.138.
[2] M.Y. Chang, H.Y. Chen, Y.L. Tsai, Temperature-controlled desulfonylative condensation of α-sulfonyl o-hydroxyacetophenones and 2-formyl azaarenes: synthesis of azaaryl aurones and flavones, J. Org. Chem. 84 (2019) 326–337, https://doi.org/10.1021/acs.joc.8b02857.
[3] H.M. Sim, C.Y. Lee, P.L. Ee, et al., Dimethoxyaurones: potent inhibitors of ABCG2 (breast cancer resistance protein), Eur. J. Pharmaceut. Sci. 35 (2008) 293–306, https://doi.org/10.1016/j.ejps.2008.07.008.
[4] A. Detsi, M. Majdalani, C.A. Kontogiorgis, et al., Natural and synthetic 2′-hydroxy-chalcones and aurones: synthesis, characterization and evaluation of the antioxidant and soybean lipoxygenase inhibitory activity, Bioorg. Med. Chem. 17 (2009) 8073–8085, https://doi.org/10.1016/j.bmc.2009.10.002.
[5] R. Haudecoeur, A. Ahmed-Belkacem, W. Yi, et al., Discovery of naturally occurring aurones that are potent allosteric inhibitors of hepatitis C virus RNA-dependent RNA polymerase, J. Med. Chem. 54 (2011) 5395–5402, https://doi.org/10.1021/jm200242p.
[6] A. Alsayari, A.B. Muhsinah, M.Z. Hassan, et al., Aurone: a biologically attractive scaffold as anticancer agent, Eur. J. Med. Chem. 166 (2019) 417–431, https://doi.org/10.1016/j.ejmech.2019.01.078.
[7] R. Liu, X. Deng, Y. Peng, et al., Synthesis and biological evaluation of novel 5,6,7-trimethoxy flavonoid salicylate derivatives as potential anti-tumor agents, Bioorg. Chem. 96 (2020), 103652, https://doi.org/10.1016/j.bioorg.2020.103652.
[8] Q. Wang, K.E. Arnst, Y. Wang, et al., Structural modification of the 3,4,5-trimethoxyphenyl moiety in the tubulin inhibitor VERU-111 leads to improved antiproliferative activities, J. Med. Chem. 61 (2018) 7877–7891, https://doi.org/10.1021/acs.jmedchem.8b00827.
[9] H.M. Sim, K.Y. Loh, W.K. Yeo, et al., Aurones as modulators of ABCG2 and ABCB1: synthesis and structure-activity relationships, ChemMedChem 6 (4) (2011) 713–724, https://doi.org/10.1002/cmdc.201000520.
[10] H. Yuan, H. Guo, X. Luan, et al., Albumin nanoparticle of paclitaxel (abraxane) decreases while taxol increases breast cancer stem cells in treatment of triple negative breast cancer, Mol. Pharm. 17 (7) (2020) 2275–2286, https://doi.org/10.1021/acs.molpharmaceut.9b01221.

[11] S. Cao, Y. Han, Q. Li, et al., Mapping pharmalogical network of multi-targeting Litchi ingredients in cancer therapeutics, Front. Pharmacol. 11 (2020) 451, https://doi.org/10.3389/fphar.2020.00451.

[12] S.N. Yamashita, Y. Tanaka, T. Kitagawa, et al., Down-regulating effect of a standardized extract of cultured lentinula edodes mycelia on cortactin in prostate cancer cells is dependent on malignant potential, Anticancer Res. 43 (3) (2023) 1159–1166, https://doi.org/10.21873/anticanres.16261.

[13] X. Li, S. He, W. Liang, et al., Marsdenia tenacissima injection induces the apoptosis of prostate cancer by regulating the AKT/GSK3β/STAT3 signaling axis, Chin. J. Nat. Med. 21 (2) (2023) 113–126, https://doi.org/10.1016/S1875-5364(23)60389-9.

[14] X. Chen, Z. Luo, X. Liu, et al., *Marsdenia tenacissima* (Roxb.) Moon injection exerts a potential anti-tumor effect in prostate cancer through inhibiting ErbB2-GSK3β-HIF1α signaling axis, J. Ethnopharmacol. 295 (2022), 115381, https://doi.org/10.1016/j.jep.2022.115381.

[15] D. Cui, Z. Luo, X. Liu, et al., Combination of metabolomics and network pharmacology analysis to decipher the mechanisms of total flavonoids of Litchi seed against prostate cancer, J. Pharm. Pharmacol. 75 (7) (2023) 951–968, https://doi.org/10.1093/jpp/rgad035.

[16] M. Chang, D. Zhu, Y. Chen, et al., Total flavonoids of Litchi seed attenuate prostate cancer progression via inhibiting AKT/mTOR and NF-κB signaling pathways, Front. Pharmacol. 12 (2021), 758219, https://doi.org/10.3389/fphar.2021.758219.

[17] A.B. Hanker, D.R. Sudhan, C.L. Arteaga, Overcoming endocrine resistance in breast cancer, Cancer Cell 37 (4) (2020) 496–513, https://doi.org/10.1016/j.ccell.2020.03.009.

[18] C.F. Almeida, N. Teixeira, A. Oliveira, et al., Discovery of a multi-target compound for estrogen receptor-positive (ER+) breast cancer: involvement of aromatase and ERs, Biochimie 181 (2021) 65–76, https://doi.org/10.1016/j.biochi.2020.11.023.

[19] R.A. Acuña, M. Varas-Godoy, D. Herrera-Sepulveda, et al., Connexin46 expression enhances cancer stem cell and epithelial-to-mesenchymal transition characteristics of human breast cancer MCF-7 cells, Int. J. Mol. Sci. 22 (22) (2021), 12604, https://doi.org/10.3390/ijms222212604.

[20] W. Xue, J. Hao, Q. Zhang, et al., Chlorogenic acid inhibits epithelial-mesenchymal transition and invasion of breast cancer by down-regulating LRP6, J. Pharmacol. Exp. Therapeut. 384 (2) (2023) 254–264, https://doi.org/10.1124/jpet.122.001189.

[21] Y. Liao, Z. Luo, Y. Liu, et al., Total flavonoids of Litchi seed attenuate stem cell-like properties in breast cancer by regulating Notch3 signaling pathway, J. Ethnopharmacol. 305 (2023) 116–133, https://doi.org/10.1016/j.jep.2023.116133.

[22] L. Li, P. Li, X. Ma, et al., Therapeutic restoring p53 function with small molecule for oncogene-driven non-small cell lung cancer by targeting serine 392 phosphorylation, Biochem. Pharmacol. 203 (2022) 115–188, https://doi.org/10.1016/j.bcp.2022.115188.

[23] X. Yun, H. Qin, B. Du, et al., Inhibitory effect and mechanism of hirsuteine on NCI-H1299 lung cancer cell lines, Oncol. Lett. 25 (5) (2023) 202, https://doi.org/10.3892/ol.2023.13788.

[24] W. Song, X. Wu, C. Cheng, et al., ARHGAP9 knockdown promotes lung adenocarcinoma metastasis by activating Wnt/β-catenin signaling pathway via suppressing DKK2, Genomics 115 (5) (2023), 110684, https://doi.org/10.1016/j.ygeno.2023.110684.

[25] A. Plangger, B. Rath, M. Hochmair, et al., Synergistic cytotoxicity of the CDK4 inhibitor fascaplysin in combination with EGFR inhibitor afatinib against non-small cell lung cancer, Invest. N. Drugs 40 (2) (2022) 215–223, https://doi.org/10.1007/s10637-021-01181-8.

[26] R. Elrayess, Y.M. Abdel Aziz, M.S. Elgawish, et al., Discovery of potent dual EGFR/HER2 inhibitors based on thiophene scaffold targeting H1299 lung cancer cell line, Pharmaceuticals 14 (1) (2020) 9, https://doi.org/10.3390/ph14010009.

[27] K. Kim, T.Y. Ryu, E. Jung, et al., Epigenetic regulation of SMAD3 by histone methyltransferase SMYD2 promotes lung cancer metastasis, Exp. Mol. Med. 55 (5) (2023) 952–964, https://doi.org/10.1038/s12276-023-00987-1.

[28] D.R. Mitteer, B.D. Greer, W.W. Fisher, et al., Teaching behavior technicians to create publication-quality, single-case design graphs in graphpad prism 7, J. Appl. Behav. Anal. 51 (4) (2018) 998–1010, https://doi.org/10.1002/jaba.483.

[29] G. Stelzer, N. Rosen, I. Plaschkes, et al., The GeneCards suite: from gene data mining to disease genome sequence analyses, Curr Protoc Bioinformatics 54 (2016), https://doi.org/10.1002/cpbi.5, 1.30.1-1.30.33.

[30] M. Safran, N. Rosen, M. Twik, R. BarShir, T. Iny Stein, D. Dahary, S. Fishilevich, D. Lancet, Practical Guide to Life Science Databases (2022) 27–56.

[31] J. Gong, C. Cai, X. Liu, X. Ku, H. Jiang, D. Gao, H. Li, ChemMapper: a versatile web server for exploring pharmacology and chemical structure association based on molecular 3D similarity method, Bioinformatics 29 (14) (2013) 1827–1829, https://doi.org/10.1093/bioinformatics/btt270, 15.

[32] P. Shannon, A. Markiel, O. Ozier, et al., Cytoscape: a software environment for integrated models of biomolecular interaction networks, Genome Res. 13 (11) (2003) 2498–2504, https://doi.org/10.1101/gr.1239303.

[33] N.R. Brown, S. Korolchuk, M.P. Martin, et al., CDK1 structures reveal conserved and unique features of the essential cell cycle CDK, Nat. Commun. 6 (2015) 6769, https://doi.org/10.1038/ncomms7769.

[34] H.M. Berman, J. Westbrook, Z. Feng, et al., The protein Data Bank, Nucleic Acids Res. 28 (2000) 235–242, https://doi.org/10.1093/nar/28.1.235.

[35] J.G. Cumming, A.M. Davis, S. Muresan, et al., Chemical predictive modelling to improve compound quality, Nat. Rev. Drug Discov. 12 (12) (2013) 948–962, https://doi.org/10.1038/nrd4128.

[36] H. van de Waterbeemd, E. Gifford, ADMET in silico modelling: towards prediction paradise? Nat. Rev. Drug Discov. 2 (3) (2003) 192–204, https://doi.org/10.1038/nrd1032.

[37] T. Hou, J. Wang, Structure-ADME relationship: still a long way to go? Expet Opin. Drug Metabol. Toxicol. 4 (6) (2008) 759–770, https://doi.org/10.1517/17425255.4.6.759.

[38] G. Xiong, Z. Wu, J. Yi, et al., ADMETlab 2.0: an integrated online platform for accurate and comprehensive predictions of ADMET properties, Nucleic Acids Res. 49 (W1) (2021) W5–W14, https://doi.org/10.1093/nar/gkab255.

[39] A. Ur-Rahman, M.I. Choudhary, S. Hayat, et al., Two new aurones from marine Brown alga spatoglossum variabile, Chem Pharm Bull 49 (2001) 105–107, https://doi.org/10.1248/cpb.49.105.

[40] M. Zhang, L. Zhang, R. Hei, et al., CDK inhibitors in cancer therapy, an overview of recent development, Am. J. Cancer Res. 11 (2021) 1913–1935. PMID: 34094661; PMCID: PMC8167670.

[41] D. Hiraoka, R. Aono, S. Hanada, et al., Two new competing pathways establish the threshold for cyclin-B-Cdk1 activation at the meiotic G2/M transition, J. Cell Sci. 129 (2016) 3153–3166, https://doi.org/10.1242/jcs.182170.

[42] O. Gavet, J. Pines, Progressive activation of CyclinB1-cdk1 coordinates entry to mitosis, Dev. Cell 18 (2010) 533–543, https://doi.org/10.1016/j.devcel.2010.02.013.

[43] M.Á. Marqués-Torrejón, E. Porlan, A. Banito, et al., Cyclin-dependent kinase inhibitor p21 controls adult neural stem cell expansion by regulating Sox2 gene expression, Cell Stem Cell 12 (2013) 88–100, https://doi.org/10.1016/j.stem.2012.12.001.

[44] D. Li, Y. Tian, Y. Ma, et al., p150 (Sal2) is a p53-independent regulator of p21 (WAF1/CIP), Mol. Cell Biol. 24 (2004) 3885–3893, https://doi.org/10.1128/MCB.24.9.3885-3893.2004.

[45] M.J. Rosendo-Pineda, J.J. Vicente, O. Vivas, et al., Phosphorylation of NMDA receptors by cyclin B/CDK1 modulates calcium dynamics and mitosis, Commun. Biol. 3 (1) (2020) 665, https://doi.org/10.1038/s42003-020-01393-3.

[46] A. Tovchigrechko, C.A. Wells, I.A. Vakser, Docking of protein models, Protein Sci. 11 (8) (2002) 1888–1896, https://doi.org/10.1110/ps.4730102.

[47] P.G. Wyatt, A.J. Woodhead, V. Berdini, et al., Identification of N-(4-piperidinyl)-4-(2,6-dichlorobenzoylamino)-1H-pyrazole-3-carboxamide (AT7519), a novel cyclin dependent kinase inhibitor using fragment-based X-ray crystallography and structure based drug design, J. Med. Chem. 51 (16) (2008) 4986–4999.

[48] D.J. Wood, S. Korolchuk, N.J. Tatum, et al., Differences in the conformational energy landscape of CDK1 and CDK2 suggest a mechanism for achieving selective CDK inhibition, Cell Chem. Biol. 26 (1) (2019) 121–130.e5.

[49] P.G. Wyatt, A.J. Woodhead, V. Berdini, et al., Identification of N-(4-piperidinyl)-4-(2,6-dichlorobenzoylamino)-1H-pyrazole-3-carboxamide (AT7519), a novel cyclin dependent kinase inhibitor using fragment-based X-ray crystallography and structure based drug design, J. Med. Chem. 51 (16) (2008) 4986–4999, https://doi.org/10.1021/jm800382h.

[50] G.H. Kuo, A. Deangelis, S. Emanuel, et al., Synthesis and identification of [1, 3, 5] triazine-pyridine biheteroaryl as a novel series of potent cyclin-dependent kinase inhibitors, J. Med. Chem. 48 (14) (2005) 4535–4546, https://doi.org/10.1021/jm040214h.

[51] A. Andreani, A. Cavalli, M. Granaiola, et al., Imidazo[2,1 -b]thiazolylmethylene- and indolylmethylene-2-indolinones: a new class of cyclin-dependent kinase inhibitors. Design, synthesis, and CDK1/cyclin B inhibition, Anti Cancer Drug Des. 15 (6) (2000) 447–452. PMID: 11716438.
[52] D. Martinez Molina, R. Jafari, M. Ignatushchenko, et al., Monitoring drug target engagement in cells and tissues using the cellular thermal shift assay, Science 341 (6141) (2013) 84–87, https://doi.org/10.1126/science.
[53] G.N. Li, X.J. Zhao, Z. Wang, et al., Elaiophylin triggers paraptosis and preferentially kills ovarian cancer drug-resistant cells by inducing MAPK hyperactivation, Signal Transduct. Targeted Ther. 7 (1) (2022) 317, https://doi.org/10.1038/s41392-022-01131-7.
[54] G. Xiong, Z. Wu, J. Yi, et al., ADMETlab 2.0: an integrated online platform for accurate and comprehensive predictions of ADMET properties, Nucleic Acids Res. 49 (W1) (2021) W5–W14, https://doi.org/10.1093/nar/gkab255.